

# Study of monolithic CMOS pixel sensors in the Belle II experiment upgrade

October 6, 2023

# Contents

<b>1 TJ-Monopix 2</b>	<b>4</b>
1.1 Matrix and flavors . . . . .	4
1.1.1 Flavors . . . . .	5
1.1.2 Pixel design . . . . .	6
1.1.2.1 Improved front-end circuit design . . . . .	7
1.2 Threshold and noise . . . . .	8
1.2.1 S-Curve method . . . . .	8
1.2.1.1 Normal FE . . . . .	9
1.2.1.2 Cascode FE . . . . .	11
1.2.1.3 HV-Cascode FE . . . . .	11
1.2.1.4 HV-Normal FE . . . . .	13
1.2.1.5 Summary Table . . . . .	14
1.2.2 Threshold dispersion and tuning . . . . .	15
1.2.2.1 First results from fine tuning . . . . .	16
1.3 ToT calibration with internal injection . . . . .	17
1.3.1 Injection circuit issues . . . . .	18
1.3.2 Time Over Threshold (TOT) curves and fit [CHECK] . .	18
1.4 Response to radioactive source and absolute calibration . . . . .	19
1.4.1 $^{55}\text{Fe}$ . . . . .	20
1.4.2 $^{241}\text{Am}$ . . . . .	22
1.4.3 $^{109}\text{Cd}$ . . . . .	22
1.4.4 Injection capacitance calibration . . . . .	22

1.4.5	Check on linearity of tot fit . . . . .	26
1.5	Operation with low threshold . . . . .	28
1.5.1	Register optimization . . . . .	28
1.5.2	Comparison between data and simulation . . . . .	29
1.5.2.1	some nice picture of the optimized thr and tuning	30
1.6	Cross talk issue and mitigation . . . . .	31
1.6.1	Hot pixel issue . . . . .	31
1.6.2	Hot pixel strategy (study) . . . . .	33
1.6.3	Cross-talk (Results) . . . . .	35
1.6.4	Mitigation . . . . .	37
1.6.4.1	Final results? . . . . .	40
1.7	Test Beam results . . . . .	40
<b>2</b>	<b>Conclusions</b>	<b>41</b>

# 1. TJ-Monopix 2

In the previous chapter we have seen the fundamental steps that had lead to the development of the CMOS MAPS sensors technology and the history of their many different prototypes.

Here we will go through the main features of TJ-Monopix 2 designed to address efficiency degradation after irradiation, one of the main issues of its predecessor Tj-Monopix 1. The characterization of the chip has crucial consequences in the VTX upgrade program and therefore in the evolution of the next OBELIX chip. The chip W14R12 (figure 1.1 on the facing page) which is one of the matrices tested during the Test Beam in Desy (July 2022) has been fully characterized in Pisa and in particular several aspects have been analyzed, among which:

- TOT calibration by internal charge injection;
- characterization with radioactive sources;
- systematic study of different registers' settings in order to operate the chip at lower thresholds;
- investigation of an important issue with cross-talk, due to digital signal from the readout, discovered trying to operate the matrix at low threshold (below  $250 e^-$ ).

This well-structured study returned relevant results which have helped in Test Beam data reconstruction and in the simulations of the upgraded VTX detector with CMOS MAPS devices.

## 1.1 Matrix and flavors

Tj-Monopix 2 is the next generation small collection electrode DMAPS prototype in TowerJazz 180 nm. The need to create a sensor capable to mantain high efficiency even after irradiation, required improvements compared to Tj-Monopix 1 in two important fields: a lower operating threshold and different pixel layout to increase charge collection efficiency all over its area, especially in the corners.

To achieve these goals, a different in-pixel front-end circuit was implemented and a lot of efforts have been focused on optimizing pixel layout in order to reduce its size, which has been decreased to  $33.04 \times 33.04 \mu m^2$  (pixel *pitch*). As a matter of fact we have seen (REFERENCE) that pixel dimensions are critical to accomplish faster charge collection across all active area, increasing

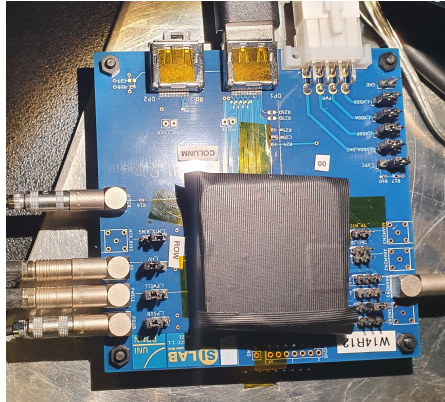


Figure 1.1: The W14R12 chip tested during the Test Beam in Desy.

the lateral electric field. For this reason it was necessary a special effort to design and create a smaller pixel but still adequate to embody the full digital readout. All of this required to work at the technology density limit and also to study for further modifications at the circuit design, such as single ended data transmission, in order to reduce the column-bus width.

The BCID bus width has been increased to 7-bits because of higher gain and higher ToT slope with respect to Tj-Monopix 1.

It's worth mentioning here that the large column height (approx. 17 mm) caused by large matrix area and the aggressive column-bus routing (which refers to the minimum line width and spacing) due to the smaller pixel size, generate a significant signal transmission delay due to the RC low pass filtering effect of the long metal wires. Consequently a special circuit has been studied that adds a variable delay to the hit pulse across the column that matches that of the BCID signal.

### 1.1.1 Flavors

The prototype is a  $2 \times 2 \text{ cm}^2$  pixel matrix which consists of 512x512 pixels and all of them are designed with a reduced deep p-well geometry (RDPW) because, as it was demonstrated during the testing of TJ-Monopix1, this type of arrangement has superior charge collection properties compared to full deep p-well coverage (FDPW) (figure 1.2 on the next page). The total active area of the matrix is approximately  $286 \text{ mm}^2$ .

As we can see in figure 1.3 on the following page, the matrix is divided in four sectors, named **flavors** that implement different variation of the front-end circuit. In the first two flavors the collection electrode is DC-coupled directly with the readout electronics, the continuous baseline reset is implemented by a forward bias diode and they differ for the pre-amplifier circuit design. The second flavor indeed, named **Cascode FE**, includes an extra-cascode transistor that increases the pre-amplifier gain which in turn leads to a 50% reduction of the threshold dispersion compared to the first flavor, the **Normal FE**. The other two flavors consist of AC-coupled pixels (through a metal-oxide-metal MOM capacitor) and in particular, the **HV-Cascode FE** also incorporates the

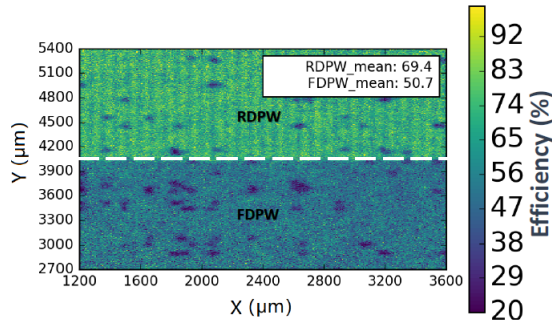


Figure 1.2: Detection efficiency map of a TJ-Monopix1 chip with  $25 \mu\text{m}$  p-eпитaxial layer that has been irradiated to  $10^{15} n_{eq}/\text{cm}^2$  NIEL.

aforementioned pre-amplifier variation. AC-coupling allows to apply an high positive bias voltage (HV) to the collection electrode, but at the same time it also causes signal losses mainly due to the additional parasitic capacitance introduced at the sensitive input node.

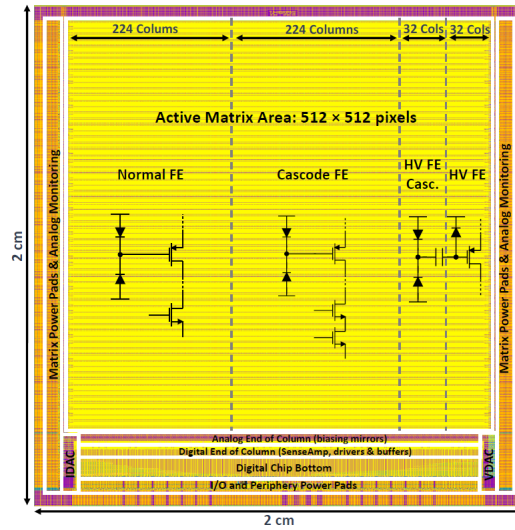


Figure 1.3: The layout of the TJ-Monopix2 prototype divided in four different flavors: **Normal**, **Cascode**, **HV-Cascode** and **HV FE**.

### 1.1.2 Pixel design

The  $2 \times 2$  pixel core layout, shown in figure 1.4 on the next page, is fully optimized and is designed in order to share as much features as possible between the four pixels. The analog area incorporates the front-end circuit, the 3-bit threshold tuning DAC and the pixel configuration registers. The digital region is composed by the 7-bit LE and TE memory (14 SRAM cells per pixel), the 10 bit address

ROM (2 bit for the pixel position inside the core and 8 for the group address), the readout control logic and the hit delay circuit that is used to correct the BCID propagation delay. Two different token signals are used to set the priority of the pixels during the readout: the *fast* one that propagates across the double column establishing the priority between the cores and the *local* one, which arbitrates the reading order of the four pixels inside each core.

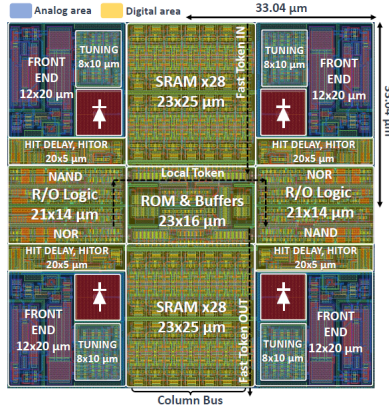


Figure 1.4: Layout of a TJ-Monopix 2 2x2 pixel core. In blue the analog area and in yellow the digital one.

### 1.1.2.1 Improved front-end circuit design

As we have seen above, there are two variations of the front-end circuit (figure on the following page), such as *normal* and *cascode* type. The latter in particular includes an extra cascode transistor which increases the pre-amplifier gain and consequently reduces the threshold dispersion.

Moreover in TJ-Monopix 2 it was preferred to incorporate a simple diode to reset the input node instead of a PMOS transistor, which was the technology implemented in TJ-Monopix 1. A side effect of this choice is that the relationship between charge injected and the ToT of the detected signal is not linear anymore, because the diode is a not linear element and its discharge rate also depends on the collected charge. Indeed in the following analysis it was necessary to fit the ToT trend with a more complex function. But at the same time, the advantages are its simplicity ( $p^+$  diffusion within the n-well collection electrode) and also the fact that it allows to increase radiation tolerance to TID effects, which was one of the key working area in the upgrade of the sensor.

In the last two AC-coupled flavors are implemented the same improvements, but here the different coupling provokes an important loss in the collected charge, as verified during the testing phase of TJ-Monopix 1 (50% losses), due at most to additional parasitic capacitances. Thus a lot of efforts have been made to improve this aspect, working on the coupling capacitor values. A signal loss of 41.5% has been reached in Tj-Monopix 2, which is a relevant enhancement with respect to its predecessor.

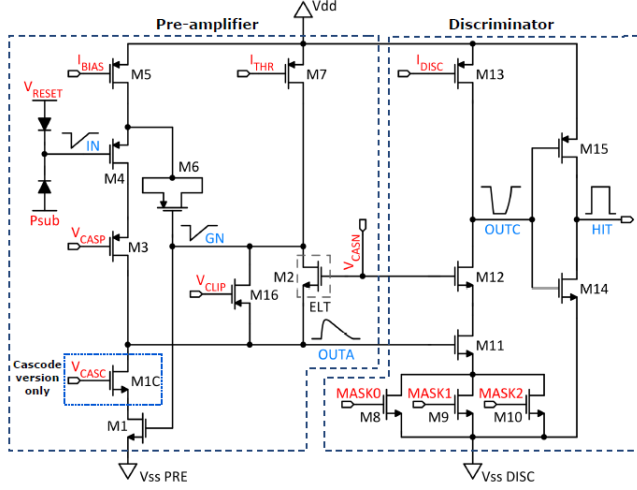


Figure 1.5: Schematic of the improved front-end circuit and its variation (extra-cascode transistor) in Tj-Monopix 2.

## 1.2 Threshold and noise

In order to achieve the absolute calibration of the whole matrix, the response of each pixel has been characterized by means of the internal charge injection.

The hit injection circuit included in TJ-Monopix 2 is similar to the one of TJ-Monopix 1. It allows to inject artificial hits through an injection capacitance  $C_{inj}$  connected at the collection electrode, which is equal to 230 aF for both the DC and AC coupling FEs. The injected charge is almost linear with the injection pulse amplitude (set by the two registers "V<sub>L</sub>" and "V<sub>H</sub>", so that  $\Delta V_{inj} = V_H - V_L$ ). Moreover the injection step is finer compare to the one of Tj Monopix 1 because of the higher voltage DAC resolution, which is indeed LSB (*Least Significant Bit*) = 7.03 mV. The injected charge resolution  $Q_{res}$  can be calculated by:

$$Q_{res} = Q_{inj} \cdot LSB = \frac{230 \text{ aF}}{q_e^-} \cdot \Delta V_{inj} = 1.4375 \frac{e^-}{mV} \cdot 7.03 \frac{mV}{DAC \text{ unit}} \approx 10.1 \frac{e^-}{DAC \text{ unit}} \quad (1.1)$$

Eventually this conversion factor has been used to convert the information of the injected charge from DAC unit to electrons unit, useful for further analysis. The four flavors have been separately analyzed to be able to study their main differences concerning their performance and features. The same method has been used for all of them, called *s-curve method* and explained below.

### 1.2.1 S-Curve method

In order to obtain the thresold and noise values for all pixels, each one of them has to be injected an arbitrary number of times (100 times in this work) for each value of the injection pulse between a minimum voltage value, chosen setting the

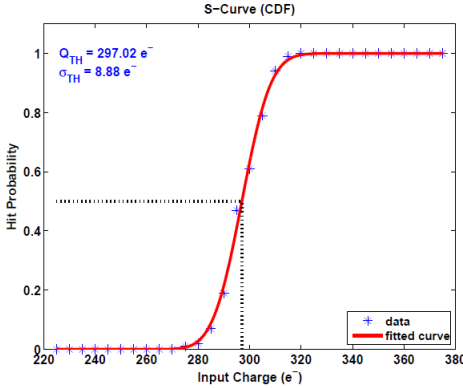


Figure 1.6: An example of the S-Curve fitted by the CDF to evaluate threshold and noise.

chip register "VL" and a maximum voltage set by the "VH" register, moving gradually with a step of 1 DAC unit (this is also adjustable). These two levels are provided by the voltage DAC.

So for each injection pulse height, the mean of 100 injection outputs are considered and it is represented as one marker in the plot. In this way, plotting the average number of detected hits in function of the injected charge, the typical curve better known as "*S-curve*" is reconstructed. It can be fit with the *Cumulative Distribution Function (CDF)*:

$$CDF(Q) = \frac{1}{2} \cdot \left( 1 + erf\left(\frac{Q - \mu}{\sigma\sqrt{2}}\right) \right) \quad (1.2)$$

from which the value of the threshold is evaluated considering the value of the injected charge at half of the curve's maximum height. Specifically the half height corresponds to a charge value for which the pixel detects 50 hits of 100 injected and so when it has an occupancy of 0.5. This information is represented by the parameter  $\mu$  obtained from the fit and the noise is evaluated from the fit parameter  $\sigma$ . The " $erf(x)$ " is the Gauss error function. In figure 1.6 is shown an example.

This method allows to study the noise and threshold of all pixels and also the threshold dispersion across an entire FE.

In the following are reported the results of this study for the flavors of all matrix, gradually injecting a charge from 0 to 140 DAC ( $\approx 1414 e^-$  adopting the conversion factor in equation 1.1)

### 1.2.1.1 Normal FE

The first flavor of the matrix is the **Normal FE**, which consist of 512 rows and 224 columns for a total of 114.688 pixels. The chip registers have been set with the same values used during the Test Beam at Desy (July 2022) which are different for the DC and AC-coupling case. They are called for simplicity "**GOE settings**" and they are reported in table 1.1 on the following page, where the different biasing voltages used to power up the chip are also added.

Registers	Normal/Cascode FE ( $P_{SUB}/P_{WELL} = -3$ V)	HV/HV-Cascode FE ( $P_{SUB}/P_{WELL} = 0$ V, HV = +5 V)
$I_{THR}$	64	30
$I_{BIAS}$	50	60
$V_{RESET}$	143	100
$I_{CASN}$	0	8
$V_{CASP}$	93	40
$V_{CASC}$	228	228
$I_{DB}$	100	100
$I_{TUNE}$	53	53
$V_{CLIP}$	255	255
$I_{COMP}$	80	80
$I_{DEL}$	88	88
$I_{RAM}$	50	50

Table 1.1: Settings of the main registers used for all flavors (W14R12 chip) during the Test Beam in Desy.

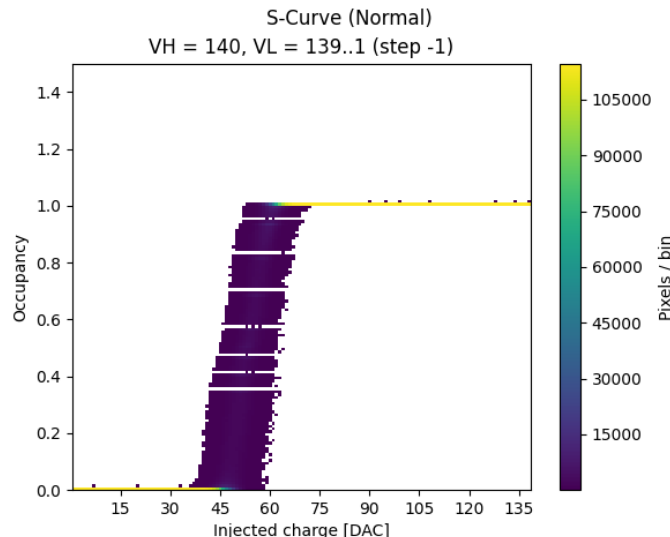


Figure 1.7: S-curves of all pixels of the Normal FE with a maximum injection pulse of 140 DAC.

Adopting this setting, none of the pixels were noisy and so it wasn't necessary to use any mask (?). In figure 1.7 are plotted all the s-curves of the all well-functioning Normal flavor pixels. The width of the plot is a first indication of the threshold dispersion of the whole flavor.

The threshold and noise distributions obtained injecting all pixels as explained above, have been fitted with a gaussian distribution and they are shown in figure on the facing page with their maps, too.

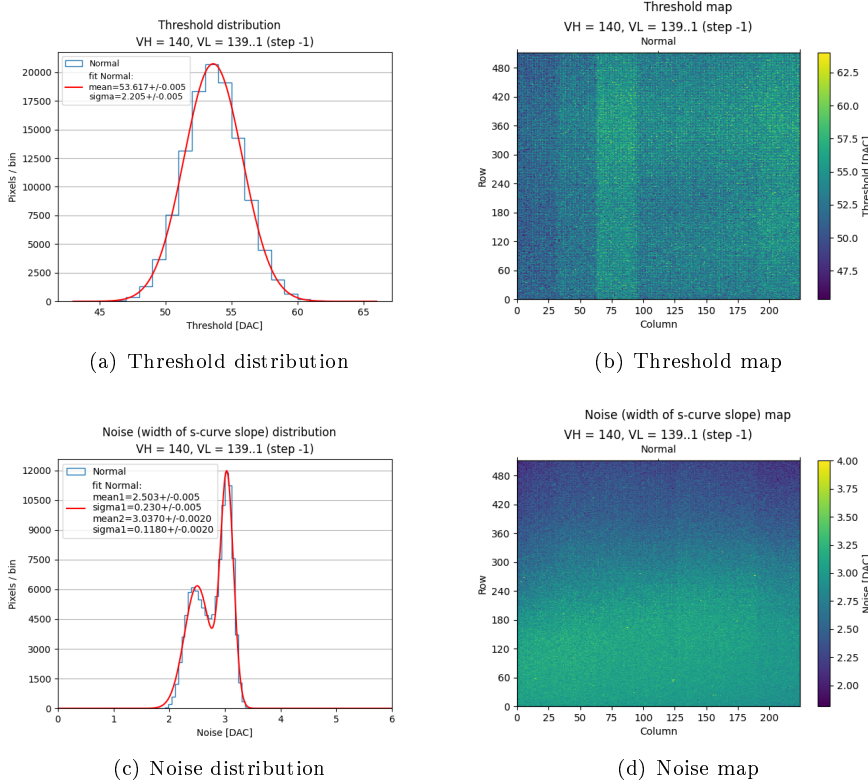


Figure 1.8: Normal FE.

### 1.2.1.2 Cascode FE

**Cascode FE** is the second flavor and like the previous one, it consists of 512 rows and 224 columns for a number of total pixels equal to 114.688. For this flavor the same procedure of Normale FE has been followed and also the same registers' values (table 1.1 on the preceding page) have been used. There were not find noisy pixels. In figure on the following page the s-curves of all pixels are shown.

The maps and the fit of the threshold and noise distributions instead, are shown in figure 1.10 on the next page.

### 1.2.1.3 HV-Cascode FE

The third flavor is **HV-Cascode FE** where HV stands for **High Voltage** and it is composed by 512 rows and 32 columns for a total number of pixel equal to 16384. Also for these last two flavors, the main chip registers are set with the same values tested and used during the Test Beam (@Desy) (but different from those used for the first two flavors). They are reported in table on the facing page .

As we can see from the plot of the alle s-curves in figure on page 13, there were a lot of noisy pixels with this choice of register settings, but at this stage of measurements they were not masked. As a matter of fact along the y-axis of

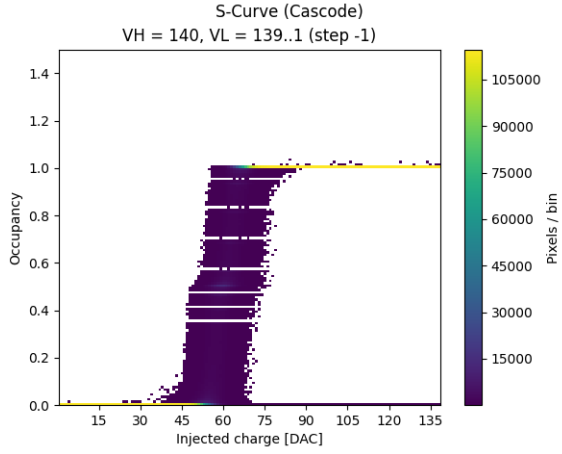


Figure 1.9: S-curves of all pixels in the **Cascade** flavor with a maximum injection pulse of 140 DAC.

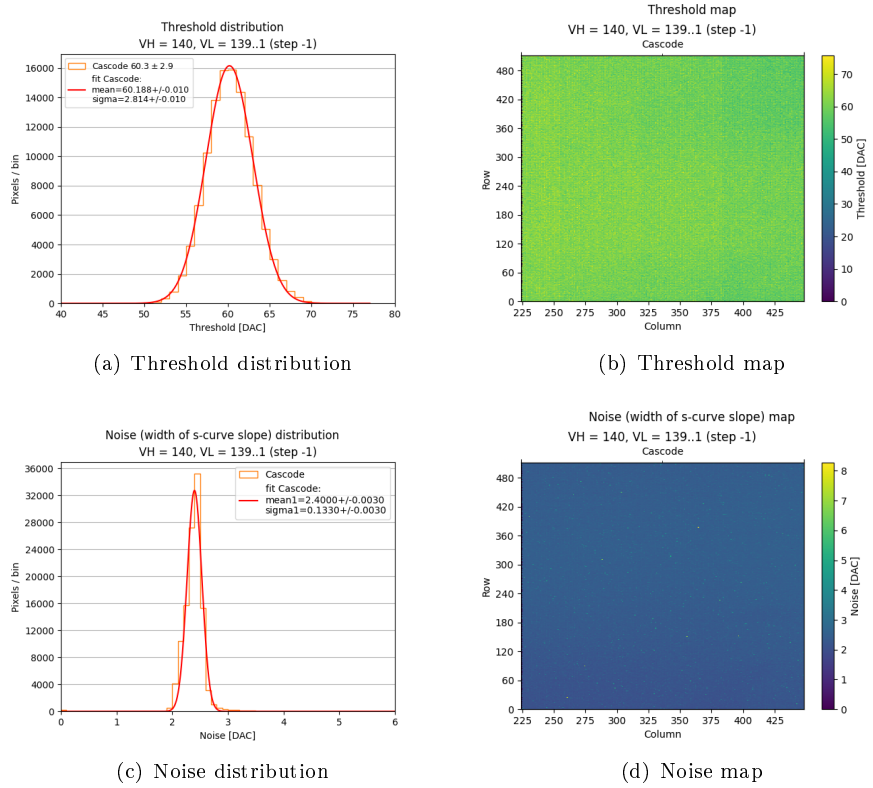


Figure 1.10: Cascode FE.

this plot is displayed the occupancy and when this value becomes higher than 1, it means that the pixel detects more hits than the injected ones, so it could

be identified as "noisy pixel" (because it results active regardless of the charge injection).

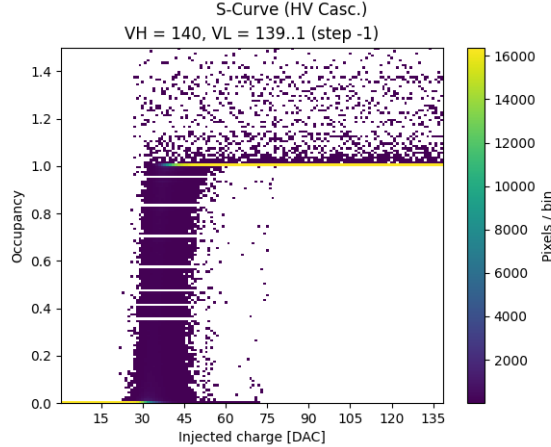


Figure 1.11: S-curves of all pixels in **HV Cascode** flavor with a maximum injection pulse of 140 DAC.

In figure 1.12 are shown the fit of the threshold and noise distributions.

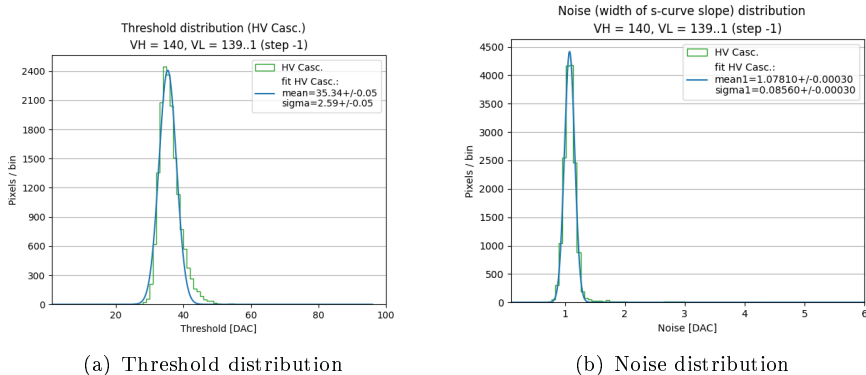


Figure 1.12: HV Cascode FE.

#### 1.2.1.4 HV-Normal FE

The fourth and last flavor is the **HV-Normal FE** which has the same layout and so the same number of pixel of the previous FE. The main registers have been set with the values reported in table on page 10. In figure on the following page, the s-curves of all pixel in this flavor. Also here we can see that there were some noisy pixels unmapped. Moreover the last 16 columns were not working (visible in the maps in figure on page 15) and as a matter of fact they had return a peak of threshold near the value 0, which is excluded from the threshold distributions plots.

So actually in this part of the matrix, the real number of pixel studied was the half of the total, such as 8192 pixels.

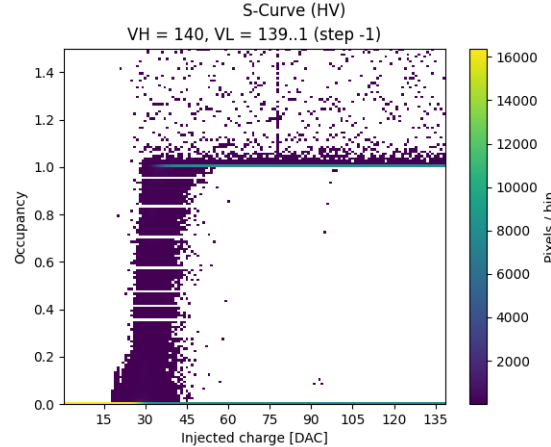


Figure 1.13: S-curves of all pixels in **HV Cascode FE** with an injection pulse of 140 DAC.

In figure 1.14 the fit of the threshold and noise distributions.

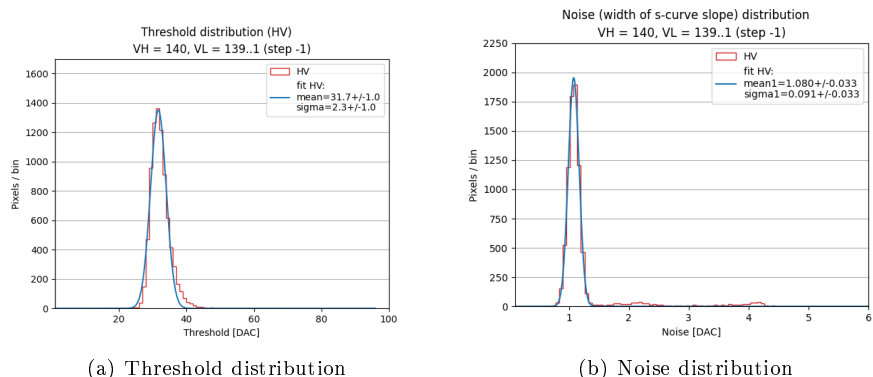


Figure 1.14: HV Normal FE.

At last in figure on the next page the threshold and noise maps of the whole HV flavor.

As we will see in the following (section on page 31), the atypical s-curves in HVs flavors have been the first hint of the cross-talk problem, tied to a global low threshold in these sectors with TB settings.

#### 1.2.1.5 Summary Table

In table on the next page a summary of results for threshold, noise and threshold dispersion of all FE.

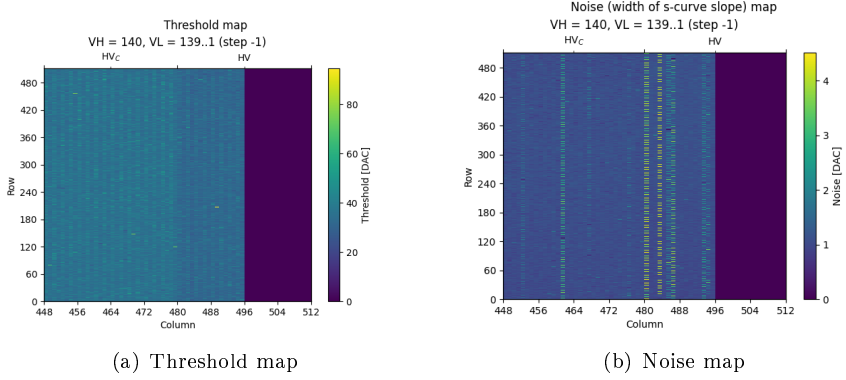


Figure 1.15: HV's FE.

Front-End	Threshold [ $e^-$ ]	Threshold dispersion [ $e^-$ ]	Noise [ $e^-$ ]
Normal	$53.62 \pm 0.01$	$2.21 \pm 0.01$	$2.503 \pm 0.005$
Cascode	$60.19 \pm 0.01$	$2.81 \pm 0.01$	$3.037 \pm 0.002$
HV - Cascode	$35.34 \pm 0.05$	$2.59 \pm 0.05$	$2.400 \pm 0.003$
HV	$31.70 \pm 0.10$	$2.30 \pm 0.10$	$1.0781 \pm 0.0003$

Table 1.2: Summary table of threshold and noise values for all flavors of the W14R12 chip.

### 1.2.2 Threshold dispersion and tuning

Despite its predecessor, Tj-Monopix 2 is equipped with a circuit which allows the *threshold tuning*. We have already mentioned that the analog part of the in-pixel front-end (figure 1.4 on page 7) includes the 3-bit threshold tuning DAC, which not only improves the global threshold dispersion across the pixels, but also solves the issue with the unintentionally masked pixels (ghost), reducing the noise even more. In other words it can adjust every pixel threshold, even if only by few DAC, in order to have a global threshold on the matrix as uniform as possible, or in any case a dispersion as small as possible, especially after irradiation. This system has been design in order to counteract some negative effects that affect the threshold dispersion like systematics (for example related to biasing), process and temperature variations and radiation damage.

Specifically the TDAC circuit, shown in figure 1.16 on the next page, helps to make threshold trimming of each pixel. This component controls the discriminator active load current  $I_{DISC}$  which is partially responsible of the pixel threshold. It works as an analog multiplexer (consisting of simple PMOS transistor switches), which selects one of seven  $I_{DISC,n}$  lines generated by the main 8-bit biasing DAC. So the possible value of the final  $I_{DISC}$  is given by the sum of two contributions:

$$I_{DISC} = I_{DISC,coarse} + (TCODE - 1) \cdot I_{DISC,fine}, \quad \text{where} \quad 1 \leq TDAC \leq 7 \quad (1.3)$$

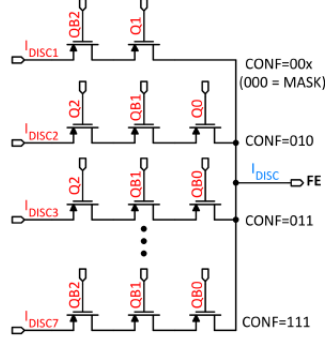


Figure 1.16: Schematic of 3-bit tuning DAC (TDAC)

$I_{DISC,coarse}$  is the current set by the primary value of threshold, resulting by the setting of the main registers which are responsible for it (mentioned after?).  $I_{DISC,fine}$  is the current selected by the fine tuning step (TDAC) and it depends on the 3-bit tuning code that is stored in the in-pixel tuning memory latch (the in-pixel configuration memory). **TCODE** is the decimal representation of the TDAC code.

For example if the 3-bit DAC are set to "111", the decimal representation is 8 and the fine tuning provide a current  $I_{DISC,7}$ , which corresponds to the highest threshold. If the 3-bit are set to "010" the corresponding TCODE is 2 and the current  $I_{DISC,1}$  is provided, which set the lowest threshold possible around the central value  $I_{DISC,coarse}$ . The particular combination "000" instead (TCODE = 0) masks the pixel by disabling the discriminator, without affecting the operation of the others.

### 1.2.2.1 First results from fine tuning

It has been trying to apply the fine tuning method to level out the threshold of some pixels as much as possible. We have considered about 12.000 pixels of the **Cascade FE** and in figure on the facing page are shown the results before and after the threshold trimming for the s-curves and threshold distributions.

As we can see the dispersion has been reduced of the 42% after the tuning and as consequence also the estimation of the threshold is more precise. In figure on page 18 are displayed the maps of the threshold and of the TDAC values, such as the value of TCODE assigned at each pixel, in order to obtain a global threshold as uniform as possible.

In more details, there are three steps for tuning:

- launch a first threshold scan through the internal charge injection, with a TDAC value equal for all pixels (usually default value is TDAC = 4).
- start a TDAC analysis which allows to choose a target threshold. During this phase, a tool tries to assign the optimized value of TDAC at each pixel in several steps, in order to get as close as possible to the set threshold. At the end it returns the final TDAC values for all selected pixels.

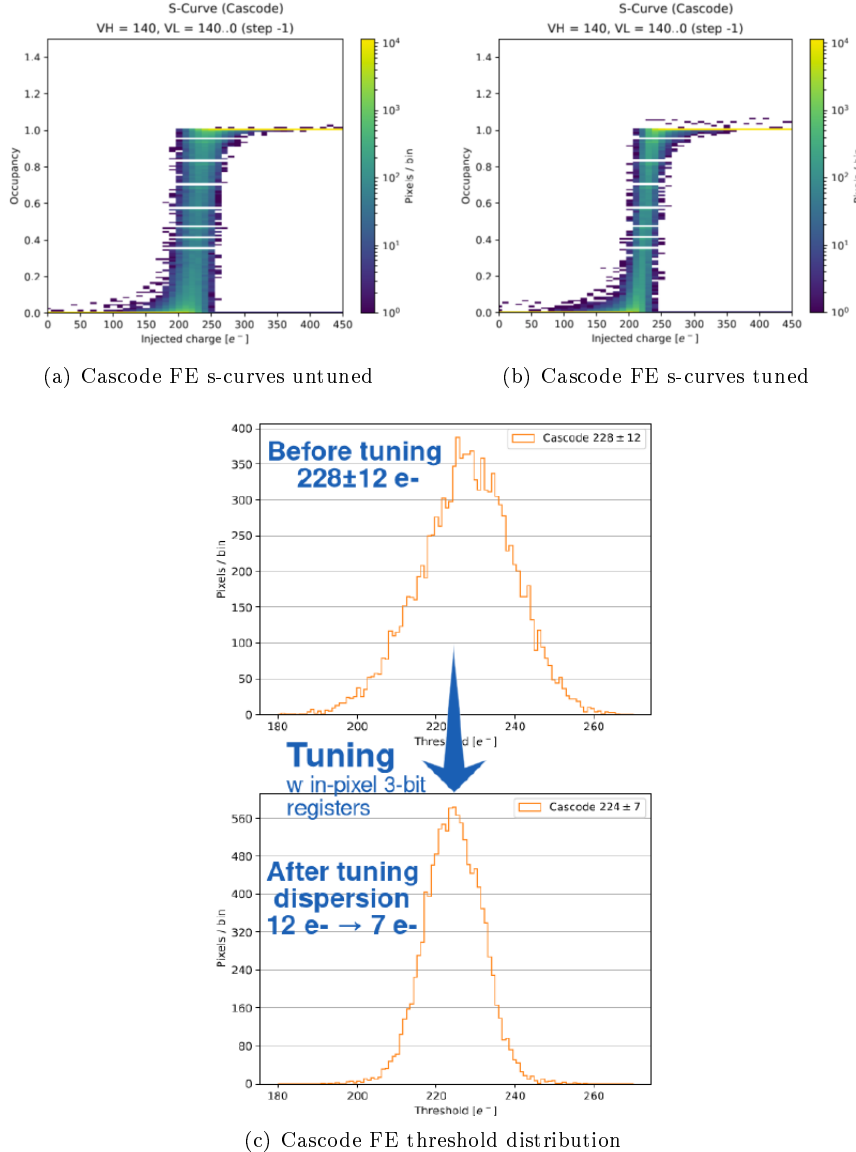


Figure 1.17: Cascode FE before tuning and after tuning comparison.

- At last another scan is launched setting the TDAC of each pixel passing the TDAC map values obtained from the previous.

### 1.3 ToT calibration with internal injection

As it has been pointed out in the previous, the choice to use a simple diode instead of a PMOS transistor as reset input baseline element, increases the tolerance to TID radiation but at the same time it implicates a non-linear re-

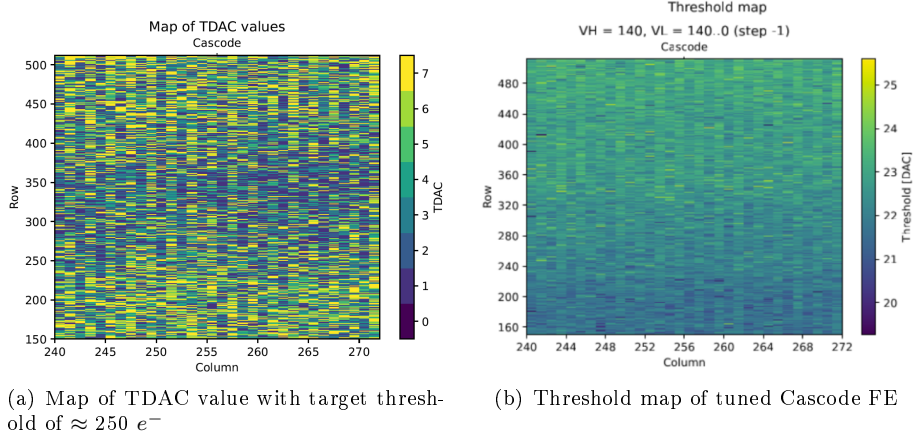


Figure 1.18: Maps of tuned Cascode FE.

lationship between the injected charge and the ToT. For this reason, one of the goal of this analysis consisted to fit the trend of  $Q_{inj}$  vs. ToT, in order to obtain the absolute calibration of the whole matrix.

### 1.3.1 Injection circuit issues

In carrying out the measurements mentioned above, we started to notice some issues with the injection circuit, which seemed to limit its working range. As a matter of fact the height of the injection pulse is expected to grow linearly increasing the value of charge to be injected. It actually happened up to a value of (about)  $\approx 140$  DAC, but for higher quantities the circuit seemed to increase not only the height of the signal, but also the threshold by a certain amount of  $\Delta V$  (or equivalently of  $\Delta Q$ , related by the conversion factor on page 8). Moreover, for injection heights grater than 200 DAC, only the threshold grows, without increasing the actual injected charge in any way.

However as we have seen in the previous section, the threshold depends on the settings of the chip registers and it can't be influenced by the injected charge, otherwise the whole response of the chip would be chaotic and it would not be reliable to take precise measurement of the impinging particles.

A method has been therefore devised to obtain reliable values of threshold and ToT up to a value of 170 DAC of effective charge injected. Moreover the characterization of the function used to describe the  $Q_{inj}$  - ToT relationship has allowed also to extrapolate ToT values in the forbidden region of charge (above  $\approx 1717 e^-$ ), where the emission peaks of the radioactive sources available in the laboratory (usually) are.

### 1.3.2 Time Over Threshold (TOT) curves and fit [CHECK]

The function chosen for this purpose is:

$$y(x) = a \cdot x + b - \frac{c}{x - t} \quad (1.4)$$

with  $a$ ,  $b$ ,  $c$  and  $t$  free parameters and where the  $y$  represents the ToT corresponding to a precise value of collected charge, express by  $x$ .

Actually we know that the ToT distribution starts to grow near the threshold, so a random parameter among them could be computed in function of the threshold value estimated from the previous measurements reported in section 1.2.1.

In more details, knowing that  $y(x_{th})$  must be equal to 0 that is the ToT value at the threshold, it can be imposed for example:

$$0 = a \cdot x_{th} + b - \frac{c}{x_{th} - t} \Rightarrow c = x_{th}^2 \cdot a + x_{th} \cdot (b - a \cdot t) - t \cdot b \quad (1.5)$$

In this way the number of parameters to fit is reduced. In principle a similar equation could be equivalently solved for  $a$ ,  $b$  and  $t$ .

So five different fits have been made: four imposing a constraint in turn on each free parameter (like shown above) and the last one leaving all parameters free. For all of them the value of  $\chi^2$  (MSE) have been computed and for all flavors it had its minimum when no parameters were fixed. So in the following the results from these last fits have been considered.

The same data collected in the previous measurements of thresholds have been used to fit the ToT curves of all pixels for each frontend. As a matter of fact we want to fully characterize the chip response with "GOE" settings (table on page 10), in order to use results for analyzing TB data. In table 1.3 are reported the results of the fits for all parameters. In figure 1.19 on the next page the plots obtained for all Normal, Cascode and HVs FE.

	<b>Normal</b>	<b>Cascode</b>	<b>HV Cascode</b>	<b>HV</b>
$a \pm \Delta a$ [ $\frac{\text{ToT}}{\text{DAC}}$ ]	$0.12 \pm 0.07$	$0.12 \pm 0.01$	$0.257 \pm 0.007$	$0.275 \pm 0.008$
$b \pm \Delta b$ [ $\text{ToT}$ ]	$4 \pm 18$	$1.4 \pm 3.1$	$3.2 \pm 1.4$	$2.3 \pm 1.6$
$c \pm \Delta c$ [ $\text{ToT} \cdot \text{DAC}$ ]	$200 \pm 1100$	$140 \pm 130$	$160 \pm 70$	$140 \pm 80$
$t \pm \Delta d$ [ $\text{DAC}$ ]	$20 \pm 90$	$40 \pm 15$	$17 \pm 6$	$13 \pm 8$

Table 1.3: Parameters obtained from the fit of ToT curve for each frontend.

## 1.4 Response to radioactive source and absolute calibration

The absolute calibration of the matrix consists in characterizing the response of each pixel to a known signal, like the emission peaks of radioactive sources. By the means of the  $Q_{inj}$  - ToT fit (section 1.3.2), it is possible to extrapolate the ToT signal value induced for whatever collected charge.

At this point then, three different X-rays radioactive sources were used to study the signal spectrum and the response time of the matrix, with emission lines from 6 to 60 KeV (corresponding approximately to 1600 and 16000 e- respectively). In fact the knowledge of the sources emission spectrum (in other words, the charge released in the matrix from particles emitted in decays) allows to compare the spectra obtained irradiating the chip, with the expected value of their peaks. It

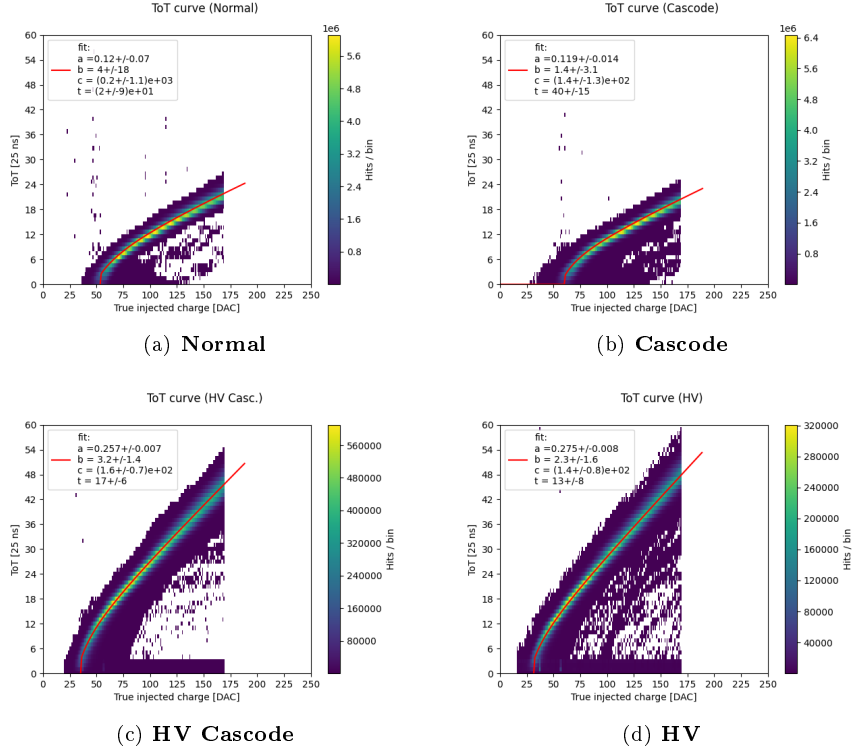


Figure 1.19: ToT curves fit for all frontend.

is worth mentioning that only the events in which all charge induced is collected in a single pixel are part of the peaks reconstructed by the chip.

In addition these radioactive sources allowed to extend the ToT calibration at higher values with respect to the limit imposed by the saturation of the internal injection circuit (section 1.3.1). In table 1.4 on the facing page are shown the emission energies of the employed sources, that it was possible to see with the chip under test.

Considering that the average energy necessary to produce an electron/hole pair in silicon is 3.65 eV, it is possible to convert the peak energies in a mean value of electrons released using the equation on the current page. So in the table are reported also the equivalent emission in electrons, which will be useful later.

$$N_{e^-} = \frac{E [eV]}{3.65 [\frac{eV}{e/h\ pair}]} \quad (1.6)$$

Now we can go through the results obtained from three different sources:  $^{55}\text{Fe}$ ,  $^{241}\text{Am}$  and  $^{109}\text{Cd}$ .

#### 1.4.1 $^{55}\text{Fe}$

The  $^{55}\text{Fe}$  source decays by **electron capture** to  $^{55}\text{Mn}$ . One of the photons emitted in this transition has an energy of 5.9 KeV ( $K_\alpha$ ) and it produces in

Source	Energy $\gamma$ [KeV]	Equivalent charge [ $e^-$ ]
$^{55}\text{Fe}$	5.9	1616
$^{241}\text{Am}$	13.9	3808
$^{241}\text{Am}$	17.7	4849
$^{241}\text{Am}$	20.7	5671
$^{109}\text{Cd}$	22	6027
$^{241}\text{Am}$	26.4	7233
$^{241}\text{Am}$	59.7	16356

Table 1.4: Emission lines of  $^{55}\text{Fe}$ ,  $^{241}\text{Am}$ ,  $^{109}\text{Cd}$  sources visible by the sensor.

turn a photo-electron which deposits a ionization charge of about  $1616 e^-$  in the sensor. All flavors were irradiate with a  $^{55}\text{Fe}$  source available in the laboratory (18 MBq). In figure 1.20 are shown the results. Each peak were fitted by a gaussian function, limited in the region of the peak itself. The shoulder visible for smaller ToT is a consequence of charge sharing among pixels.

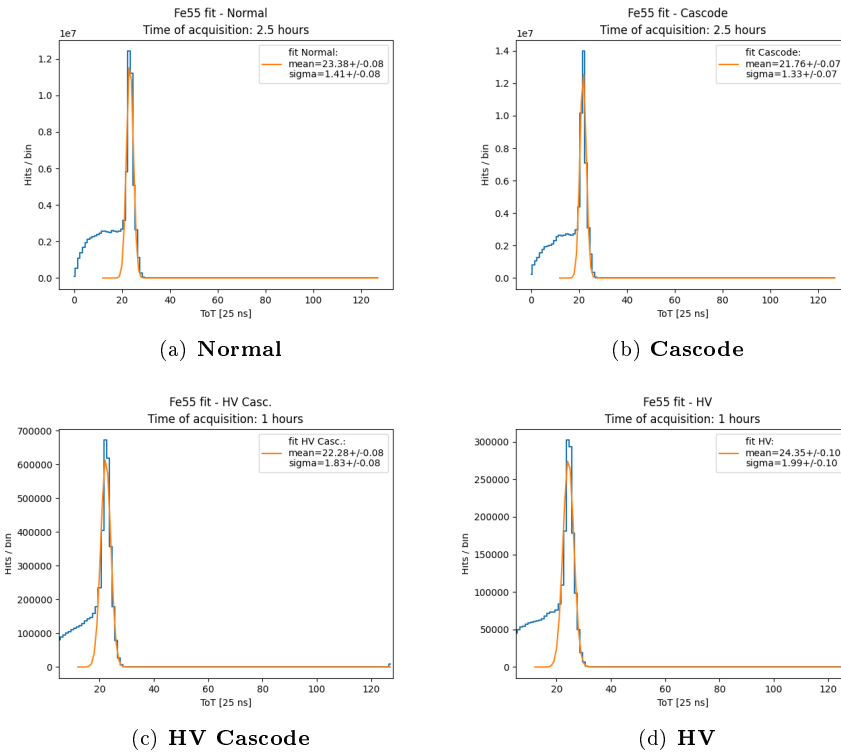


Figure 1.20:  $^{55}\text{Fe}$  peaks for all frontends.

As it can be seen for the HV's FE a cut has been applied only to make clearly visible the emission line, indeed a lot of noisy pixels caused a sharp peak

at 0 ToT. As a matter of fact in this flavors there were several columns of not-functioning pixels. In the box of each plot are also reported the results of the fit that will be crucial in the following.

### 1.4.2 $^{241}\text{Am}$

The  $^{241}\text{Am}$  source has a more complex spectrum (figure 1.21) and not all its peaks can be detected by the chip (because of the limited range of ToT available, depending on the number of bits dedicated to it). The spectrum shows other minor peaks besides the usual intense gamma peaks (59.5 and 26.3 keV) and several characteristic L X-rays from  $^{237}\text{Np}$  (20.7, 17.7 and 13.9 keV).

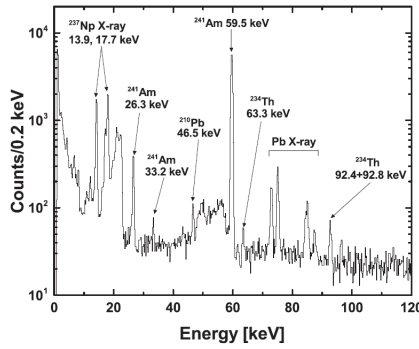


Figure 5. Gamma-ray spectrum of the  $^{241}\text{Am}$  source.

Figure 1.21:  $^{241}\text{Am}$   $\gamma$  emission spectrum.

Results are reported in figure 1.22 on the facing page.

In the case of the first two flavors, it could be possible to fit four peaks of the emission lines. In case of the HV's flavors instead, only three peaks for the HV-Cascode FE and two for the HV. As already discussed (section on page 7) the AC-coupling causes about 41.5% of signal loss, so they are much less evident and more difficult to fit as isolated peak.

### 1.4.3 $^{109}\text{Cd}$

The third source employed was the  $^{109}\text{Cd}$ . This isotope decays into  $^{109}\text{Ag}$  by electronic capture, producing a photon of 22 KeV in the transition. In figure on page 24 the results obtained irradiating all FEs.

### 1.4.4 Injection capacitance calibration

Here it is necessary to point out that for iron source more statistics were collected so in this case a complete analysis of each pixel has been done. For the other sources instead, there weren't enough statistics on every pixel so the injection capacitance has been estimated only as a mean value for the whole front-end, just to compare with the results obtained from the iron analysis.

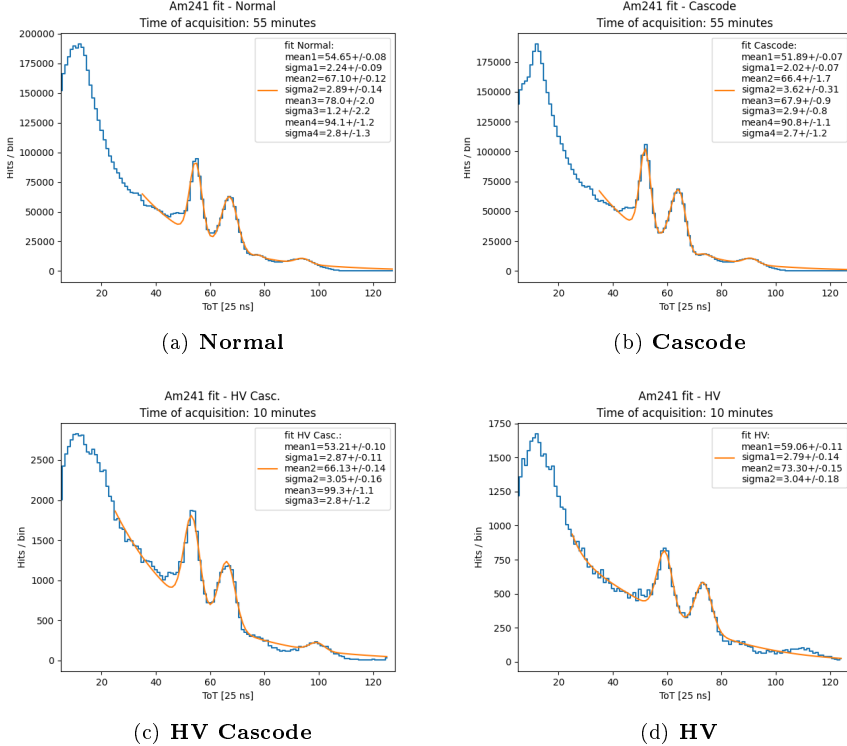


Figure 1.22:  $^{241}\text{Am}$  peaks for all frontends.

In case of  $^{55}\text{Fe}$  source, we managed to fit the emission peak for each working pixel of the whole matrix. The value of the charge corresponding to the ToT peak of the emission line was extrapolate considering the parameters' values obtained by fitting the  $Q_{inj}$  - ToT relationship (section on page 18).

Specifically the fit function on page 18 was inverted obtaining:

$$x(y) = \left( \frac{t}{2} - \frac{b}{2a} + \frac{y}{2a} \right) \pm \sqrt{\left( \frac{t}{2} + \frac{b}{2a} - \frac{y}{2a} \right)^2 + \frac{c}{a}} \quad (1.7)$$

where  $x$  represents the charge corresponding to the ToT labeled by  $y$ .

As shown in table on page 21, the charge released in the sensor (considering that collected from only one pixel) corresponds roughly to  $1616\text{ e}^-$ . Therefore it was possible to estimate the conversion factor for each pixel as follows:

$$C_f \left[ \frac{e^-}{DAC} \right] = \frac{1616\text{ e}^-}{ToT \frac{DAC}{ToTunit}} \quad (1.8)$$

By these steps, a value of the injection capacitance was estimated for each well-functioning pixel. In figure on page 25 is reported the distributions of the injection capacitance estimated, fitted by a gaussian function.

Regarding the other sources, it was impossible to fit the distributions for each pixel due to low statistics. For this reason only a mean value for all flavor

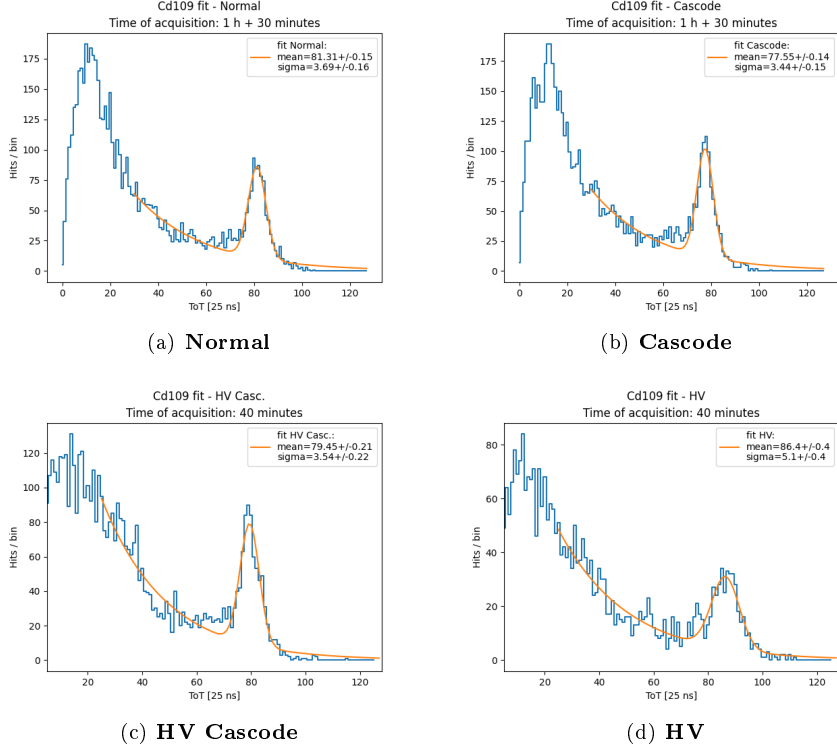


Figure 1.23:  $^{109}\text{Cd}$  pekas for all frontends.

could be extrapolate. In table on the current page the results obtained with the same method used with the iron source, but considering all pixels of each flavor.

Source peak	$C_{Normal}$	$C_{Cascode}$	$C_{HV\,Cascode}$	$C_{HV}$
$^{55}\text{Fe}$ (5.9 KeV)	9.37	9.00	19.33	18.56
$^{241}\text{Am}$ (13.9 KeV)	8.94	8.91	19.23	18.22
$^{241}\text{Am}$ (17.7 KeV)	9.16	8.84	19.59	18.63
$^{241}\text{Am}$ (20.7 KeV)	9.15	10.11	-	-
$^{109}\text{Cd}$ (22 KeV)	9.32	9.39	20.16	19.6
$^{241}\text{Am}$ (26.4 KeV)	9.60	9.61	19.25	-
Mean value	9.26	9.31	19.51	18.75

Table 1.5: Estimation of injection capacitance of all flavors for different source emission peaks.

Bringing equation on page 8 back to mind, the conversion factors of the flavors are not those expected. In particular for the HV's flavors, they are almost the double and it could mean that the injection capacitance is greater than expected. But as mentioned in section on page 8, the prototype under

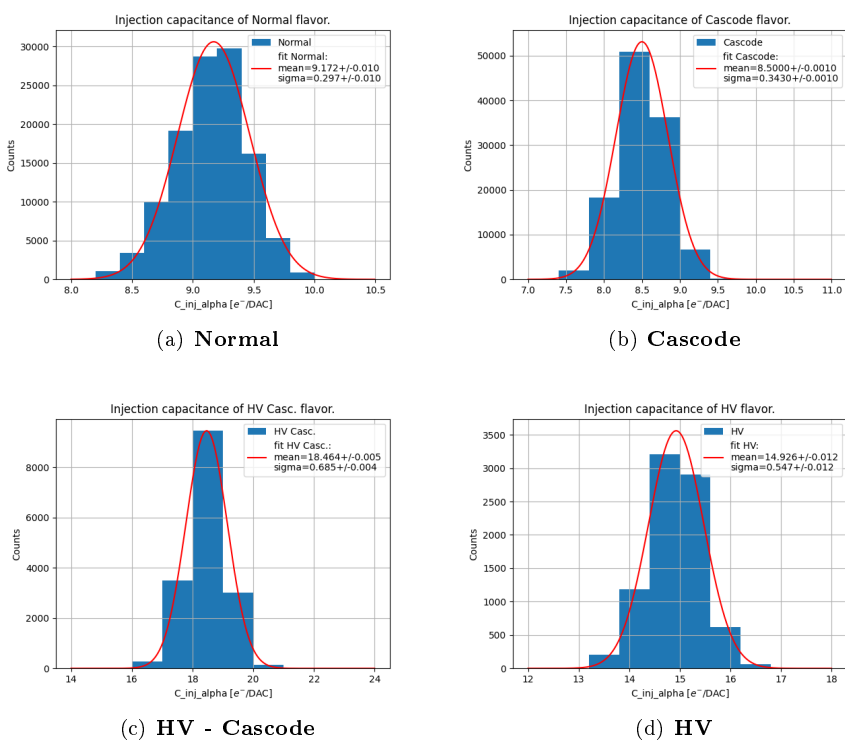


Figure 1.24: Injection capacitance distributions of all FE.

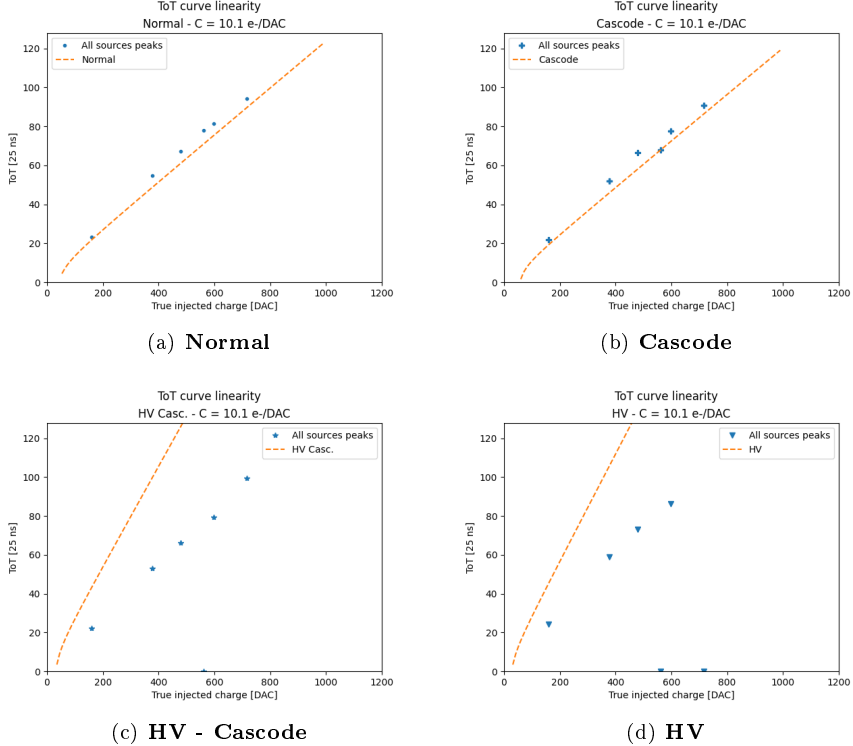


Figure 1.25: ToT linearity of all flavors assuming the nominal(expected) conversion factor equal to  $10.1 \frac{e^-}{DAC}$ .

test was designed in order to have the same injection capacitance for all flavor, equal to 230 aF (despite this doesn't seem to be the case). In fact the cause of the different results for the conversion factors might be due also to the expected loss of the collected charge for HV FEs (section on page 7).

#### 1.4.5 Check on linearity of tot fit

Eventually the value of all emission peaks (obtained by the fit) from the several sources have been plotted for each frontend in order to verify the agreement between their trend and the ToT-Q relationship studied by the internal injection.

Initially the average quantity of electrons expected to be released for each peak, has been calculated with the nominal conversion factor equal to  $10.1 \frac{e^-}{DAC}$ . As it could be seen from results in figure on the current page there isn't good agreement between data and ToT relationship studied in section on page 18.

After the calibration instead, assuming the average value of injection capacitance (*Mean value*) reported in table on page 24, the charge corresponding to the emission peaks have been recalculated and results are shown in figure on the facing page.

As we can see, a better agreement is therefore obtained and this shows that through calibration we are now able to interpret data with greater precision,

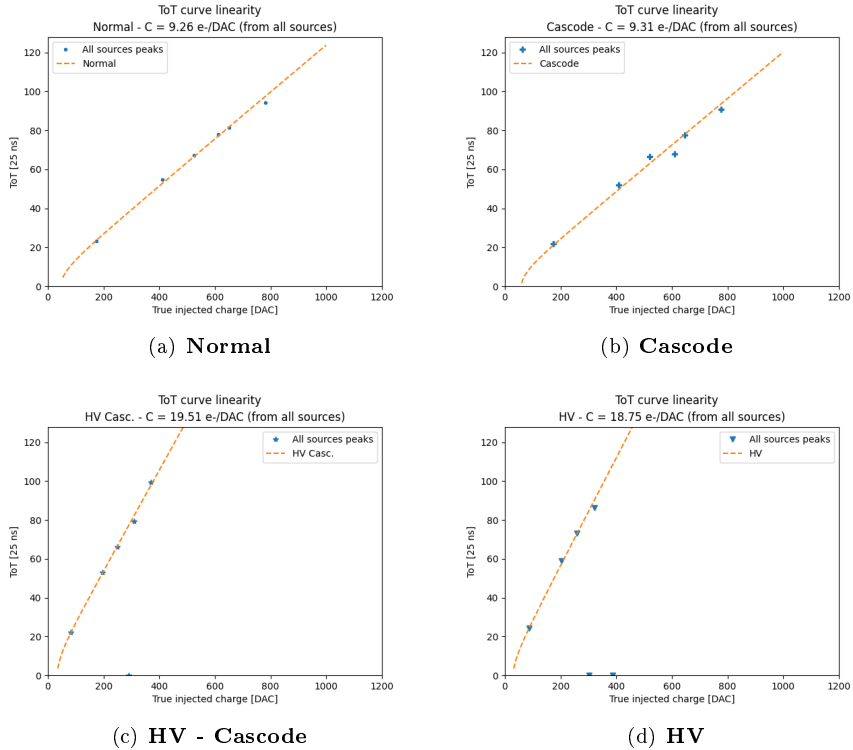


Figure 1.26: ToT linearity of all flavors assuming the conversion factor obtained from calibration for each FE.

which was the main purpose of this analysis.

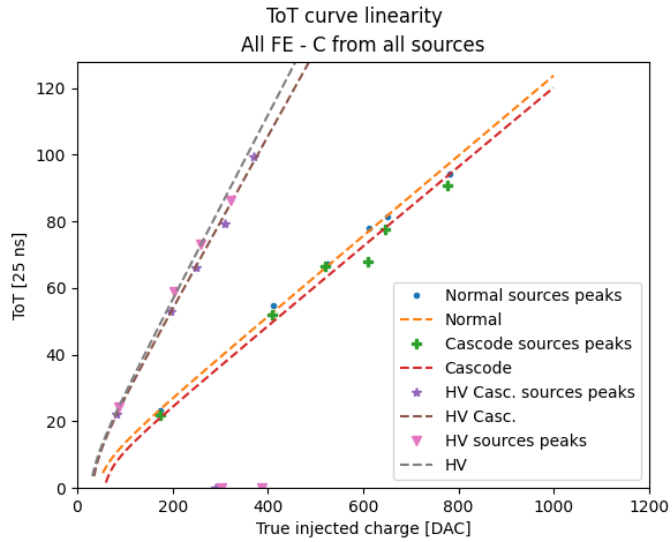


Figure 1.27: Summary of trends.

## 1.5 Operation with low threshold

One of the most important target in sensor design is to keep high efficiency even after irradiation damages. All experimental environments indeed, are exposed to high doses of radiations, so it's crucial to ensure the functionality of the detectors, even after being irradiated.

For this reason, many tests were done in order to understand the chip behaviour at low threshold where a good value of efficiency could be preserved. Moreover working at low threshold allowed to detect low charge events due to charge sharing or charge trapping (effect which increases after irradiation), especially in case of thin epitaxial material.

### 1.5.1 Register optimization

As we have seen in section (REFERENCE), there are a lot of registers which control the discriminator threshold and also the readout sequence. So preliminary it was necessary to explore their possible settings in order to operate the chip at low threshold.

Now we will go through the main registers used for this purpose, in order to explain their functionality. There are several dozens of registers but we focused on some of the most important and crucial to set the threshold and its dispersion:

- $I_{CASN}$  : this current is responsible of the output baseline signal. In particular it sets the baseline of the FE output that goes to the input discriminator. In a few words, higher this value, higher the baseline, lower the threshold and also a little bit the gain and vice versa by decreasing it.
- $I_{THR}$ : it controls the pre-amplifier feedback strength and speed, so it is responsible for the output reset rate. Increasing this current increases the gain and the time that the analog output takes to get back to the baseline and as consequence, it increases a lot the maximum value of the ToT. In fact it is recommend to set  $I_{THR}$  to low value (e.g. 8 nA[ref]) in order to avoid high ToT slope.
- $I_{DB}$ : this current corresponds to  $I_{DISC,coarse}$  explained in section 1.2.2 on page 15. It represents the primary current that sets the discriminator threshold, to which another current is added by the tuning.
- $I_{TUNE}$ : it corresponds to  $I_{DISC,fine}$  instead (always section on page 15). Remembering the equation from tuning<sup>1</sup> (on page 15), this is the current to multiply by the TDAC value, which is added to  $I_{DB}$ , during the tuning process.
- $I_{BIAS}$ : this current acts on the pre-amplifier input transistor and influences the threshold dispersion and the gain. In particular increasing this value, the dispersion decreases and the gain becomes greater. Nevertheless it can't be increased a lot because it affects the power consumption, too.

---

<sup>1</sup>

$$I_{DISC} = I_{DISC,coarse} + (TCODE - 1) \cdot I_{DISC,fine}, \quad \text{where} \quad 1 \leq TDAC \leq 7 \quad (1.9)$$

- $V_{RESET}$ : this register influences the threshold dispersion. Lowering its value, the dispersion decreases and vice versa.

### 1.5.2 Comparison between data and simulation

In the interest of understanding how the registers' setting of the chip influences the threshold, several measurements have been taken with different configuration of their values. The results are compared with simulations done by Hung Pham. (...). [???]

$I_{CASN}$

In figure 1.28, we can see the simulated behaviour of the threshold and the gain, increasing the value o  $I_{CASN}$ .

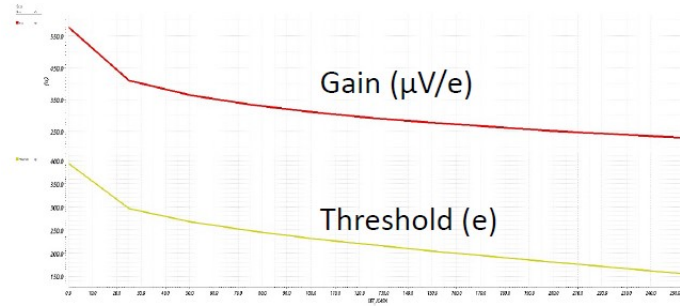


Figure 1.28: Trends of Gain and Threshold increasing  $I_{CASN}$ .

To verify the trend of threshold as this current varies, three different acquisitions have been taken by fixing  $I_{THR} = 20, 40, 64$  and increasing  $I_{CASN}$  from 0 to 30 DAC, with a step of 5 DAC. We have done this enabling 200 pixels in the Cascode FE (rows: 472 - 512, cols: 225 - 230).[??]

Each threshold distribution has been fitted with a gaussian function in order to estimate the average threshold value and its dispersion.

In figure 1.29 on the next page are reported all trends obtained.

$I_{THR}$

Reusing the same data of the previous measurements, the trend of the threshold have been studied bt changing the value of  $I_{THR}$  and fixing that of  $I_{CASN}$ . In this case only  $I_{CASN}$  from 0 to 15 DAC is considered, because for higher values we don't have enough measures of the threshold (specifically only two for  $I_{THR}=40, 64$ ). The results are shown in figure 1.30 on the following page.

As expected, increasing  $I_{THR}$  results to lower gain and faster return to baseline, so higher threshold. We can compare them with the simulation shown in figure 1.31 on page 31.

**Time over Threshold (ToT)**

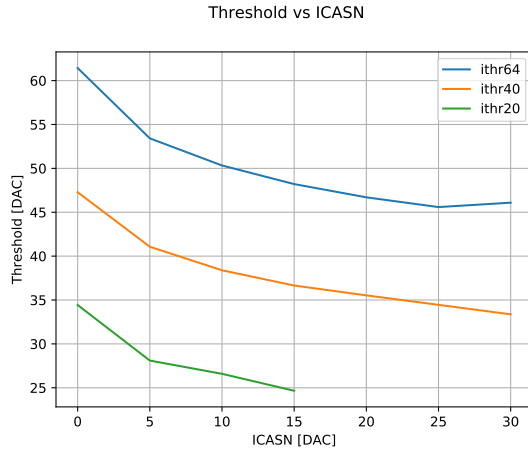


Figure 1.29: Threshold vs.  $I_{CASN}$  for  $I_{THR}= 20, 40, 64$ .

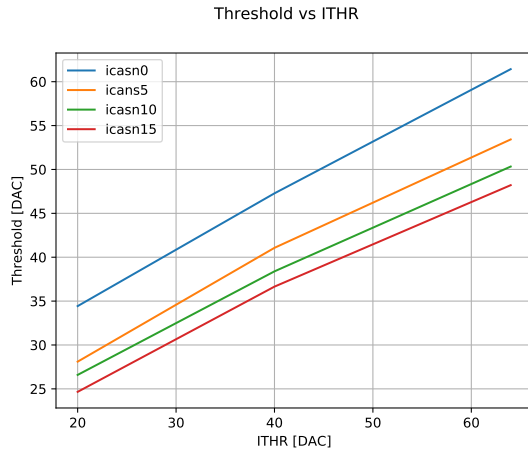


Figure 1.30: Threshold vs.  $I_{THR}$  for  $I_{CASN}= 0, 5, 10, 15$ .

The last analysis done to make a comparison with the simulations, is about the trend of the ToT changing the value of  $I_{CASN}$  for a fixed value of  $I_{THR}$  and vice versa. In particular we consider the data obtained with  $I_{CASN}$  fixed to 0 DAC and  $I_{THR}$  to 64 DAC, which are the values studied and used for these registers during the Test Beam in Desy.

Results are reported in figure on page 32 and on page 33. Also here we can see a good agreement between data and simulations.

### 1.5.2.1 some nice picture of the optimized thr and tuning

!!!!

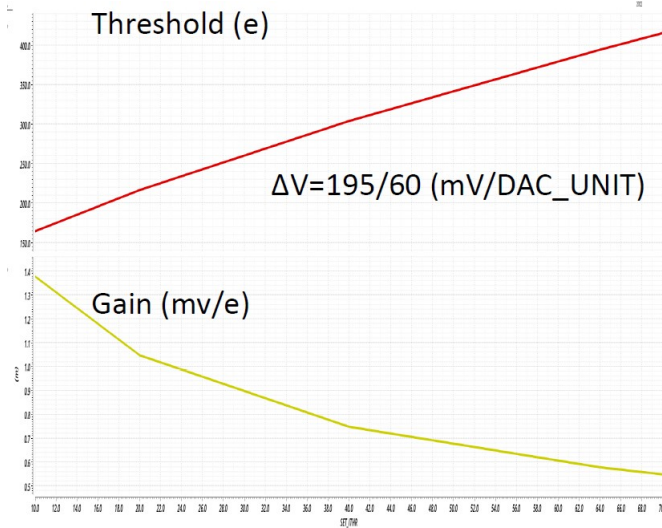


Figure 1.31: Trends of Gain and Threshold increasing  $I_{CASN}$ .

## 1.6 Cross talk issue and mitigation

As it was already pointed out, during the measurements of the average threshold of all FEs, there were something atypical in the s-curves of the HV flavors (subsection 1.2.1.4 on page 13), indeed some pixels seem to have occupancy greater than 1. This behavior threatens the good functionality of the overall matrix response, because these *noisy pixels* flood the readout, giving unreliable results.

Also the systematic study of different registers' configurations has revealed the presence of the hot pixels which has prevented to use certain settings and as consequence to reach lower global thresholds.

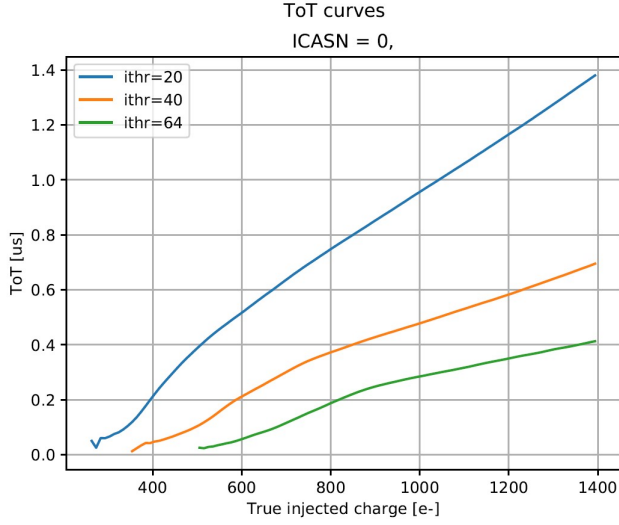
For this reason an investigation has been conducted in order to understand the reasons why they start to fire and how to cure them as far as possible. In the meantime an important issue with cross-talk of the readout signals was discovered, and so in this section we examine this effect and some attempts to mitigate it using different settings/bias.

### 1.6.1 Hot pixel issue

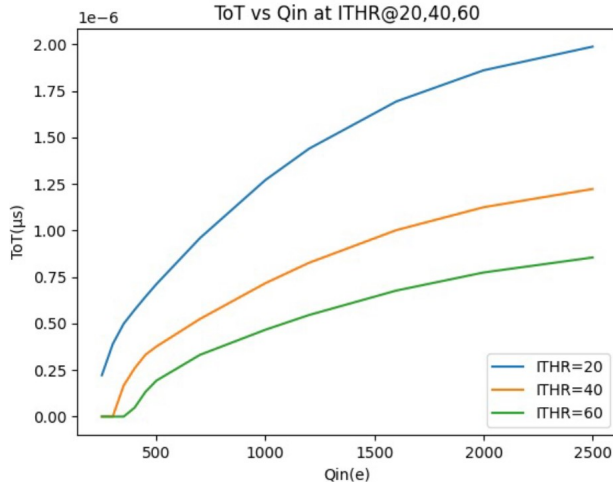
First of all we noticed that in the s-curves of the HV flavors (e.g. that of HV-Cascode reported in figure on page ??), the atypical behavior could be triggered by a digital signal sent to the matrix during the readout activity at low threshold. This consideration is based on two main reasons:

- when the matrix has high threshold, like for Normal and Cascode FE, all pixels seem to behave as expected, without *hot pixels*.

Lowering the threshold and running some source acquisitions without any source, no strange behaviour was observed. Acquiring data with a radioactive source instead, even Normal and Cascode FE seem to reveal the



(a) ToT vs  $I_{THR}$  ( $I_{CASN}=0$  DAC) - Data (Cascode)

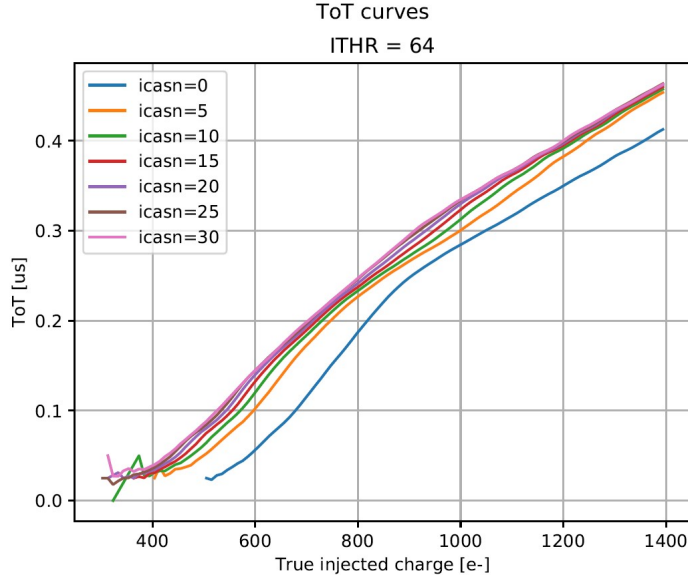


(b) ToT vs  $I_{THR}$  ( $I_{CASN}=0$  DAC) - Simulation

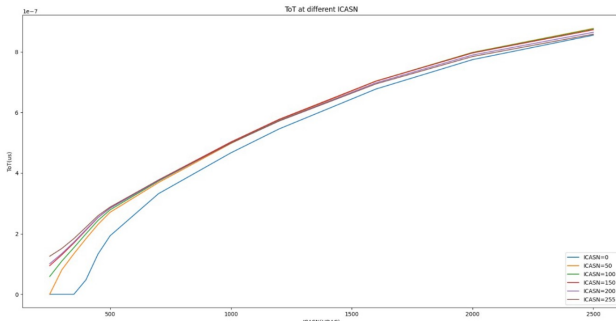
Figure 1.32: ToT vs  $I_{THR}$

same problem. This led to thinking that during the readout of good pixels an induced signal is created which couples with some other pixels, in particular with those at lower threshold with respect to the average value. If the height of this signal exceeds the threshold of the single pixel, it causes some spurious hits, making the pixel "hot".

- Moreover, always considering the HV Cascode s-curves, it could be noticed that in the region before the threshold ( $Q_{inj} < \text{threshold}$ , pointed by the blue arrow) there isn't an anomalous activity which means that the induced signal is not due to the BCID that is always sent to the matrix during the injection or an acquisition with the source, regardless of being above



(a) ToT vs  $I_{CASN}$  ( $I_{THR}=64$  DAC) - Data (**Cascode**)



(b) ToT vs  $I_{CASN}$  ( $I_{THR}=64$  DAC) - Simulation

Figure 1.33: ToT vs  $I_{CASN}$

or below the threshold. The atypical behaviour indeed, is in the region above the threshold ( $Q_{inj} > \text{threshold}$ , pointed by the red arrow) where the occupancy of some pixels becomes greater than 1. This means that these *hot pixels* detect more hits of those injected.

From these first observations, we have reached the conclusion that the cross talk could be tied to the readout activity. So we have started investigating the timestamp of those hits not synchronize with the timestamp of the injection.

### 1.6.2 Hot pixel strategy (study)

At first, it has been lowered the threshold in order to "create" hot pixel also in the first two flavors of the matrix. In fact with TB settings the threshold was too high and the hypothetical induced signal didn't caused spurious hits. For

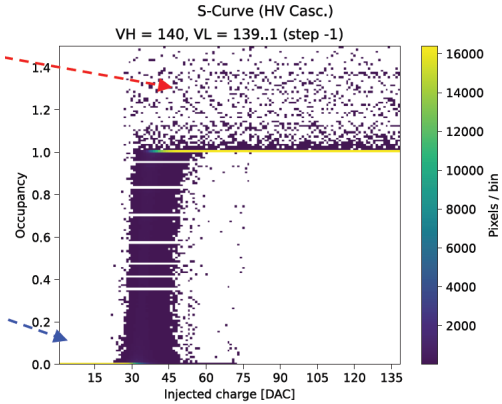


Figure 1.34: HV-Cascode s-curves.

this purpose different settings were tried, changing some fundamental registers responsible for the threshold like those listed and explained on page 28.

Then several tests have been run under controlled conditions:

- one healthy(good) pixel was injected;
- one *hot pixel* (two or three in different tests) was enabled but not injected;
- the all matrix except these pixels was disabled.

In this way (remembering the readout sequence [REFERENCE]) the readout cycle had a known duration and two different timing info (and some precautions) had been used to study the induced signal with greater precision:

- $\Delta TS$  (TimeStamp) between two consecutive hits: the TimeStamp is assigned from the FPGA when the TOKEN rises on the TE of the first hit to read, but only if the previous readout frame is completed. So, if the hit coming from a *hot pixel* is after the hit from the injected one, the minimum  $\Delta TS$  has to be equal to the readout time of 1 pixel and so to the duration of the FREEZE\_STOP signal.  
This info has allowed to verify if the hot pixel fires after the good injected one or not.
- LE(hit) - TE(previous hit): this quantity measures the elapsed time between a hit and the previous one. This is a finer info than the  $\Delta TS$  because it allows to correlate the hit with the induced digital signal, originate from the readout cycle.

Moreover, since a 7-bit BCID is sent to the matrix during its activity, it was important to keep short ( $<128$  clock cycle) the duration of the full readout sequence and to not enable too many pixels in order to not extend too much the readout frame. Otherwise the information on the leading edge of the pixel could not be correlated with the token of the previous hit. In other words, if the readout frame exceed 128 clock cycles, since the token could be raised if the matrix is **not** freeze, even if an hit is arrived before it could be read only in

the next frame when it could rise again the token, but in this case it will have different TimeStamp. So in this case the TS is useless for our purpose.

### 1.6.3 Cross-talk (Results)

Referring to the readout sequence, in order to understand which signal could induce cross talk, each register value has been moved one by one. In table on the current page just an example from the several settings tried is reported.

Register	Value
FREEZE_START_CONF	10
READ_START_CONF	13
READ_STOP_CONF	15
LOAD_CONF	30
FREEZE_STOP_CONF	31
STOP_CONF	31

Table 1.6: Register values of the Readout cycle.

Doing so indeed, the LE-TE info has to shift by the same value with which the signal that cause the cross talk has been changed. This step of the procedure is tied with the necessity to keep the readout sequence within the maximum 128 BCID range.

For example, if FREEZE\_START\_CONF is responsible for the cross talk signal, we expected that shifting its value by a certain amount, the hot pixels start to fire after that this signal arises due to the hit on the injected pixel. So the value of LE-TE has to be FREEZE\_START\_CONF + some potential delay. Same argument for the other registers.

By this procedure, repeated for each readout register, we have come to the conclusion that the cross-talk could be related to the raising and falling edge of the FREEZE signal.

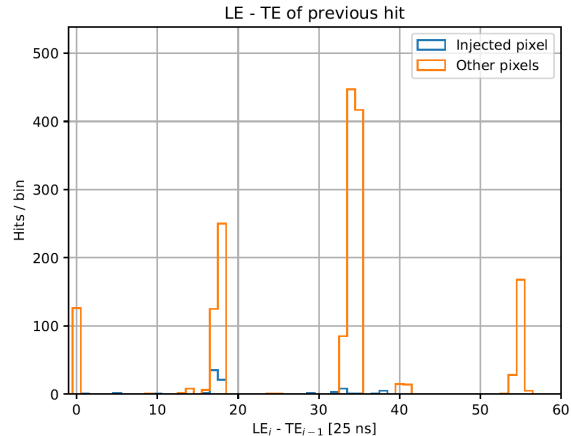
In figure on the following page an example of some results obtained. It is the histogram of the time last between the leading edge of an hit and the trailing edge of the previous hit, when one pixel is injected and two are read. It's possible to see several peaks (referring to the readout setting reported in table on the current page):

- one at 0, that represent the situation in which both hits come from hot pixel firing simultaneously after the injection. This means that they are activated by the same signal and so it is the most important confirmation that is cross-talk and not random firing pixel signal;
- one at  $\approx 18$  equal to FREEZE STAR raising + 8  $\rightarrow$  first induced signal;
- one at  $\approx 35$  equal to FREEZE STOP falling + 4  $\rightarrow$  second induced signal;
- one at  $\approx 55$  equal to FREEZE STOP falling + 4 when two different pixels are read. In more details, after the first 30 time unit until the first

LOAD CONF, a distinct pixel reading starts and it takes another 20 time unit (LOAD - FREEZE START) + 1 unit time to conclude the frame with the FREEZE STOP and so  $51 + 4$  unit time wrote above. Therefore when two pixels are read, the FREEZE STOP falls after 51 clock cycles, and it is compatible with the last peak in the plot.

Injected pixel: (217, 140) Other pixels: [(218, 155) (222, 188)] Assuming timestamp clock = 40.00 MHz Green = injected pixels							
Row	Col	LE	TE	ΔLE	ΔTE	ΔTS[25ns]	TS[25ns]
140	217	12	29	124	123	5627.0000	635972.0000
140	217	8	25	124	124	5628.0000	641600.0000
155	218	60	60	52	35	35.0000	641635.0000
188	222	59	60	127	0	0.0000	641635.0000
155	218	115	115	56	55	55.0000	641690.0000
188	222	114	115	127	0	0.0000	641690.0000
155	218	42	43	56	56	55.0000	641745.0000
188	222	42	42	0	127	0.0000	641745.0000
140	217	4	21	90	107	5482.0000	647227.0000

(a) An example of the time quantity used in the analysis.



(b) An example of the LE(hit)-TE(previous hit) histogram.

Figure 1.35: Some results of the cross-talk studies.

As already stated, we run several tests varying the number of pixels to read, the value of the readout registers, different combination of hot and good pixels and also different spatial location of them in the matrix to exclude the possibility that the problem was related to particular columns. All results are in agreement with the interpretation explained above.

MAH...

Furthermore it has been tried to estimate the height of the induced signal from the threshold of the hot pixel. For this reason we have tried different setting of the currents cited above to make a pixel *hot* in order to understand when the induced signal went above the threshold. We have found that the signal could (may) correspond to  $100/150 e^-$ .

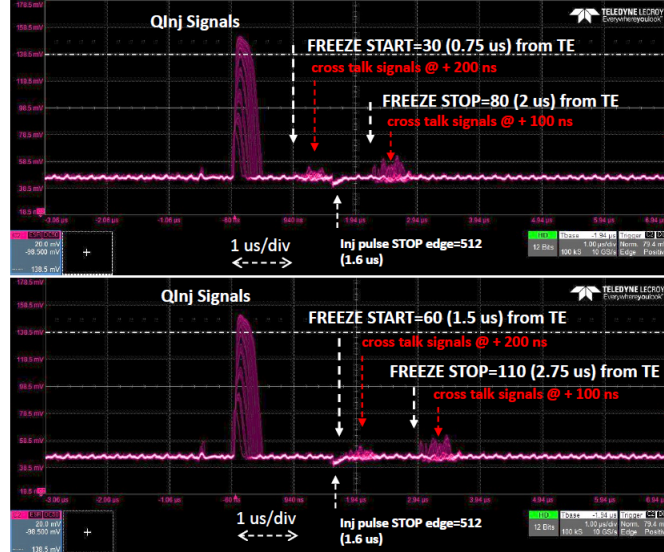


Figure 1.36: Cross-talk of the FREEZE signal on oscilloscope's analog output, for different value of FREEZE\_START\_CONF register.

In figure on this page an analog acquistion of the readout signals taken by an oscilloscope.

In these tests one pixel was injected from 0 to 140 DAC (in the acquisition it can be seen in the increasing signal height). There are two different group of spikes, the first which smaller and represent the cross-talk from the raising of the FREEZE signal and the second, larger and corresponding to the cross talk from the falling edge of the same signal. Moreover it's possible to see that in the two different pictures, the cross talk signals move according to the different settings of the FREEZE START/STOP edge.

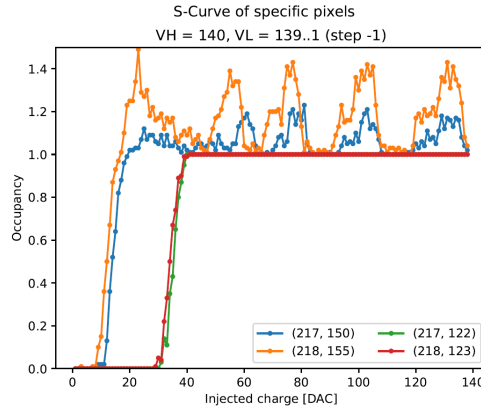
#### 1.6.4 Mitigation

As seen in the previous, the problem of the hot pixel is tied to the induction signal produced during the readout which cause cross-talk. It becomes more important(significant, serious) when there is grater dispersion threshold.

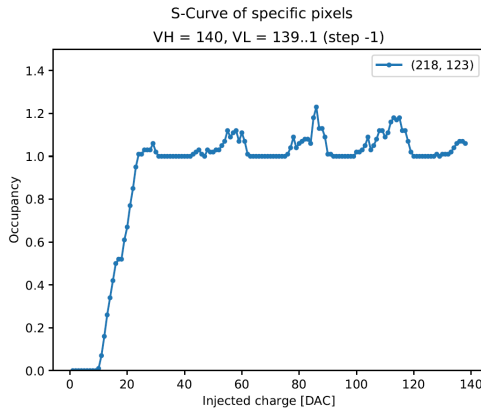
Potentially every pixel could become *hot* if its threshold is lower than the height of the cross-talk signal since the FREEZE is sent across the entire matrix.

As an example in figure on page ?? it si possible to compare the behaviour of pixel (218, 123) changing(modifying) some registers' values in order to reduce the threshold.

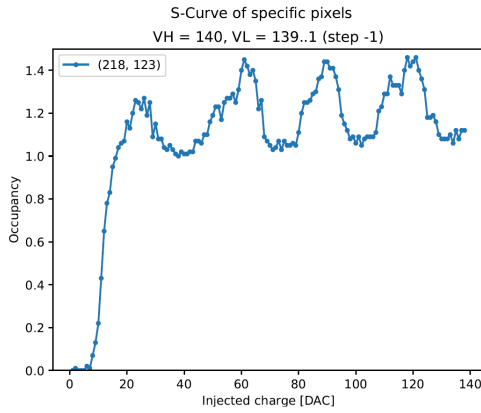
For this reason, a possible treatment could be related to the threshold tuning, explained in section (reference) , which could allow to make the pixels threshold more uniform (less threshold dispersion) and simultanously targeting a value greater than the induced signals.



(a)  $I_{DB}=100, I_{TUNE}=53$  - Good behavior



(b)  $I_{DB}=60, I_{TUNE}=150$  - Pixel starts to misbehave



(c)  $I_{DB}=55, I_{TUNE}=150$  - Pixel becomes *hot*

Figure 1.37: S-curve of the pixel (218, 123) for different register settings.

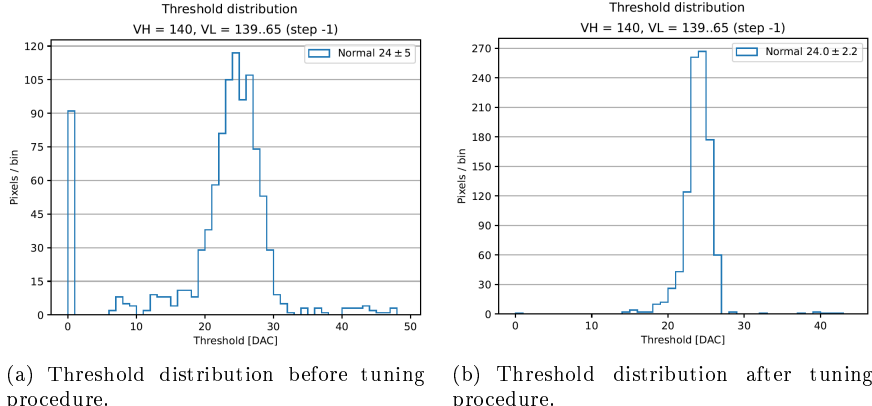


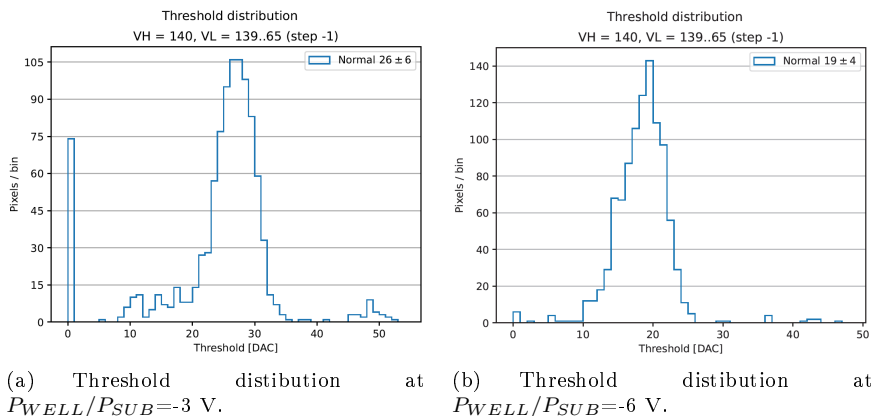
Figure 1.38: Threshold tuning to reduce hot pixels.

In figure on this page an example of the results obtained.

It's evident the reduction of the tail in the threshold distribution, in fact the dispersion is reduced by 56%. Also the hot pixels decrease from 18% to 1.2% of the total number of pixels studied. [We can notice indeed that the peak at 0 threshold disappears.]

Moreover it has been tried to increase the voltage bias of the all matrix, too. We remember that all previous test has been run with  $P_{WELL}/P_{SUB}$  set to -3 V. This value was increased to -6 V and indeed there were some improvements. In fact increasing the bias, we expected a decrease of the diode capacitance thus higher gain and lower threshold dispersion. In addition the coupling with the cross talk signal is reduced too and so the induced signal height.

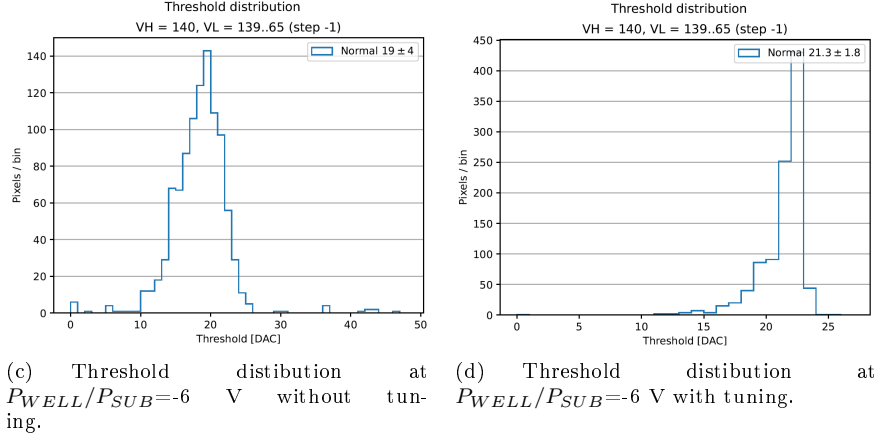
In figure on the current page a comparison between the threshold distribution respectively at -3 V and -6 V, with same registers setting and without tuning.



At higher bias voltage not only is the threshold lower (higher gain), but also its dispersion, as expected. And despite that there are fewer hot pixels: 1.3% at -6V against 17% at -3 V. Also here it's clear a reduction of the threshold distribution tail.

#### 1.6.4.1 Final results?

Eventually the final results obtained with both threshold tuning and a bias voltage on  $P_{WELL}/P_{SUB} = -6$  V.



As we can see in figure on this page, the threshold dispersion decreases with the number of hot pixels. In fact without tuning there are 1.3% of them, instead with tuning procedure there are none at all.

## 1.7 Test Beam results

Hit detection efficiency from bespin article

## 2. Conclusions

# List of Figures

1.1	The W14R12 chip tested during the Test Beam in Desy. . . . .	5
1.2	Detection efficiency map of a TJ-Monopix1 chip with $25 \mu\text{m}$ p-epitaxial layer that has been irradiated to $10^{15} n_{eq}/cm^2$ NIEL. . . . .	6
1.3	The layout of the TJ-Monopix2 prototype divided in four different flavors: <b>Normal</b> , <b>Cascode</b> , <b>HV-Cascode</b> and <b>HV FE</b> . . . . .	6
1.4	Layout of a TJ-Monopix 2 2x2 pixel core. In blue the analog area and in yellow the digital one. . . . .	7
1.5	Schematic of the improved front-end circuit and its variation (extra-cascode transistor) in Tj-Monopix 2. . . . .	8
1.6	An example of the S-Curve fitted by the CDF to evaluate threshold and noise. . . . .	9
1.7	S-curves of all pixels of the Normal FE with a maximum injection pulse of 140 DAC. . . . .	10
1.8	Normal FE. . . . .	11
1.9	S-curves of all pixels in the <b>Cascode</b> flavor with a maximum injection pulse of 140 DAC. . . . .	12
1.10	Cascode FE. . . . .	12
1.11	S-curves of all pixels in <b>HV Cascode</b> flavor with a maximum injection pulse of 140 DAC. . . . .	13
1.12	HV Cascode FE. . . . .	13
1.13	S-curves of all pixels in <b>HV Cascode FE</b> with an injection pulse of 140 DAC. . . . .	14
1.14	HV Normal FE. . . . .	14
1.15	HV's FE. . . . .	15
1.16	Schematic of 3-bit tuning DAC (TDAC) . . . . .	16
1.17	Cascode FE before tuning and after tuning comparison. . . . .	17
1.18	Maps of tuned Cascode FE. . . . .	18
1.19	ToT curves fit for all frontend. . . . .	20
1.20	$^{55}\text{Fe}$ peaks for all frontends. . . . .	21
1.21	$^{241}\text{Am}$ $\gamma$ emission spectrum. . . . .	22
1.22	$^{241}\text{Am}$ peaks for all frontends. . . . .	23
1.23	$^{109}\text{Cd}$ pekas for all frontends. . . . .	24
1.24	Injection capacitance distributions of all FE. . . . .	25
1.25	ToT linearity of all flavors assuming the nominal(expected) conversion factor equal to $10.1 \frac{e^-}{DAC}$ . . . . .	26
1.26	ToT linearity of all flavors assuming the conversion factor obtained from calibration for each FE. . . . .	27
1.27	Summary of trends. . . . .	27

1.28 Trends of Gain and Threshold increasing $I_{CASN}$	29
1.29 Threshold vs. $I_{CASN}$ for $I_{THR} = 20, 40, 64$	30
1.30 Threshold vs. $I_{THR}$ for $I_{CASN} = 0, 5, 10, 15$	30
1.31 Trends of Gain and Threshold increasing $I_{CASN}$	31
1.32 ToT vs $I_{THR}$	32
1.33 ToT vs $I_{CASN}$	33
1.34 HV-Cascode s-curves.	34
1.35 Some results of the cross-talk studies.	36
1.36 Cross-talk of the FREEZE signal on oscilloscope's analog output, for different value of FREEZE_START_CONF register.	37
1.37 S-curve of the pixel (218, 123) for different register settings.	38
1.38 Threshold tuning to reduce hot pixels.	39

## List of Tables

1.1	Settings of the main registers used for all flavors (W14R12 chip) during the Test Beam in Desy. . . . .	10
1.2	Summary table of threshold and noise values for all flavors of the W14R12 chip. . . . .	15
1.3	Parameters obtained from the fit of ToT curve for each frontend. . . . .	19
1.4	Emission lines of $^{55}\text{Fe}$ , $^{241}\text{Am}$ , $^{109}\text{Cd}$ sources visible by the sensor. . . . .	21
1.5	Estimation of injection capacitance of all flavors for different source emission peaks. . . . .	24
1.6	Register values of the Readout cycle. . . . .	35